AD-A116 967 NAVAL RESEARCH LAB WASHINGTON DC F/G 17/9
TRACKING CLOSELY SPACED MULTIPLE SOURCES VIA SPECTRAL-ESTIMATIO--ETC(U)
JUN 82 W F GABRIEL
UNCLASSIFIED NRL-8603 NL

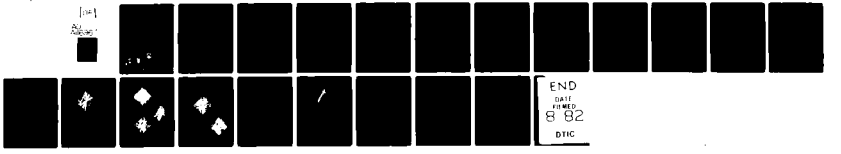

END
DATE FILMED
8 82
DTIC

NRL Report 8603

Tracking Closely Spaced Multiple Sources via Spectral-Estimation Techniques

WILLIAM F. GABRIEL

Electromagnetics Branch
Radar Division

June 23, 1982

NAVAL RESEARCH LABORATORY
Washington, D.C.

SECURITY CLASSIFICATION OF THIS PAGE (When Data Entered)

REPORT DOCUMENTATION PAGE	READ INSTRUCTIONS BEFORE COMPLETING FORM
1. REPORT NUMBER: NRL Report 8603	2. GOVT ACCESSION NO.: AD-A116 967
	3. RECIPIENT'S CATALOG NUMBER:
4. TITLE (and Subtitle): TRACKING CLOSELY SPACED MULTIPLE SOURCES VIA SPECTRAL-ESTIMATION TECHNIQUES	5. TYPE OF REPORT & PERIOD COVERED: Interim report on a continuing NRL problem.
	6. PERFORMING ORG. REPORT NUMBER:
7. AUTHOR(s): William F. Gabriel	8. CONTRACT OR GRANT NUMBER(s):
9. PERFORMING ORGANIZATION NAME AND ADDRESS: Naval Research Laboratory, Washington, DC 20375	10. PROGRAM ELEMENT, PROJECT, TASK AREA & WORK UNIT NUMBERS: 61153N; RR0210543; NRL Problem 53-0624-0-2
11. CONTROLLING OFFICE NAME AND ADDRESS: Office of Naval Research, Arlington, VA 22217; Naval Air Systems Command, Washington, DC 20361	12. REPORT DATE: June 23, 1982
	13. NUMBER OF PAGES: 20
14. MONITORING AGENCY NAME & ADDRESS(if different from Controlling Office)	15. SECURITY CLASS. (of this report): UNCLASSIFIED
	15a. DECLASSIFICATION/DOWNGRADING SCHEDULE:

16. DISTRIBUTION STATEMENT (of this Report)

Approved for public release; distribution unlimited.

17. DISTRIBUTION STATEMENT (of the abstract entered in Block 20, if different from Report)

18. SUPPLEMENTARY NOTES

19. KEY WORDS (Continue on reverse side if necessary and identify by block number)

Adaptive arrays
Antennas
Nonlinear processing
Spectral analysis
Tracking
Digital processing

Accession For
NTIS GRA&I
DTIC TAB
Unannounced
Justification
By
Distribution/
Availability Codes
Dist Avail and/or Special
A

DTIC COPY INSPECTED 3

20. ABSTRACT (Continue on reverse side if necessary and identify by block number)

Modern spectral-estimation techniques have achieved a level of performance that attracts interest in applications areas such as the tracking of multiple spatial sources. In addition to the original "superresolution" capability, these techniques offer an apparent "absence of sidelobes" characteristic and some reasonable solutions to the difficult radar coherent-source problem that involves a phase-dependent SNR (signal-to-noise ratio) penalty. This report reviews the situation briefly, and it discusses a few of the techniques that have been found useful, including natural or synthetic doppler shifts, non-Toeplitz forward-backward subaperture-shift processing, and recent
(Continued) cont

DD FORM 1 JAN 73 1473 EDITION OF 1 NOV 65 IS OBSOLETE
S/N 0102-014-6601

SECURITY CLASSIFICATION OF THIS PAGE (When Data Entered)

20. ABSTRACT (Continued)

eigenvalue/eigenvector analysis algorithms. The techniques are applied to multiple-source situations that include mixtures of coherent and noncoherent sources of unequal strengths, with either an 8- or a 12-element linear-array sampling aperture. The first test case involves the estimation of six sources, two of which are 95% correlated. The second test case involves a tracking-simulation display example of four moving sources: three are -10-dB coherent sources 95% correlated, and the other is a strong 20-dB noncoherent source. These test cases demonstrate the remarkable improvements obtained with the recent estimation techniques, and they point to the possibilities for real-world applications.

CONTENTS

TRACKING CLOSELY SPACED MULTIPLE SOURCES VIA SPECTRAL-ESTIMATION TECHNIQUES

INTRODUCTION

The tracking of closely spaced multiple coherent spatial sources is a problem area in the field of radar where current spectral estimation techniques may find some application. Interest is stimulated by two important performance characteristics reported for these techniques [1]:

- "Superresolution" which implies the resolution of two or more sources within the conventional beamwidth of an RF antenna aperture; and
- "Absence of sidelobes" which implies the resolution of two or more sources of unequal strengths when those sources are spaced more than a beamwidth apart.

Both of these advantages accrue because the Fourier-transform convolution of the conventional antenna-aperture window function is avoided; it is replaced by a spatial-filter-function multiplication [2]. The spatial filter is data adaptive to the source scenario, using the available degrees of freedom of the system in an optimal LMS (least-mean-square) error sense. *Both characteristics are restricted* to those applications where the processing system has sufficient degrees of freedom to model the source scenario and the sources have sufficient signal-to-noise ratio (SNR) to be distinguished. Also, both terms should be used with caution to avoid misinterpretation with respect to the conventional radar system definitions of resolution and sidelobes, thus the quotation marks are used.

If the RF sources in the far field are truly noncoherent, that is, if their signals have a zero correlation coefficient at the antenna aperture, then impressive resolution performance is obtainable via many of the optimal estimation algorithms and techniques described in the literature. These would include the maximum entropy method (MEM) of J. P. Burg [2], the maximum likelihood method (MLM) of J. Capon and R. T. Lacoss [2], the Wiener sample covariance matrix inverse (SMI) filter and its several equivalent techniques [1-4], the autoregressive (AR) least squares methods of A. H. Nuttall and L. Marple [5,6], the eigenvalue/eigenvector analysis techniques of R. L. Schmidt and of E. Bienvenu and L. Kopp [7,8], and others [9].

However, if the RF sources in the far field happen to be coherent, as is often the case in radar situations, then the resolution performance vs SNR for the above algorithms and techniques will be degraded, often to the point of complete failure of resolution. This degradation in performance has been addressed by several researchers [10-12], and some particularly interesting and constructive results have recently been reported by Massachusetts Institute of Technology's Lincoln Laboratory [13]. This report reviews briefly the nature of the coherent-source problem, discusses several of the useful current techniques, and applies the techniques to multiple-source situations which include both coherence and unequal strengths in order to help illustrate their potential advantages. All results in this report are derived from computer simulations based upon the digital signal samples described in the appendix.

Manuscript submitted March 22, 1982.

THE COHERENT-SOURCE PROBLEM AND SOME SOLUTIONS

The resolution of coherent radio-frequency (RF) spatial sources (or equivalent radar targets) is more difficult for these nonlinear adaptive processing techniques, basically because correlated signals produce fields that are nonstationary in space [10,11]. To address the problem of coherency, consider the aperture-modulation envelope function produced by two equal-strength coherent sources located 8° apart in the far field, as illustrated in Fig. 1. This envelope function is produced by the interaction of the two coherent plane wavefronts along the line containing the aperture-sampling elements, and it is easily derived by computation of the averaged sample covariance matrix term for the kth and lth elements. Using the signal sample notation described in the appendix and an overbar to denote averaging, and assuming zero correlation between receiver noise and the far-field sources, we may write

$$\overline{(E_k^* E_l)} = \overline{|\eta_k^* \eta_l|} + \bar{A}_1^2 e^{ju_1(x_l - x_k)} + \bar{A}_2^2 e^{ju_2(x_l - x_k)} + 2\overline{A_1 A_2} \cos\,[u_d(x_l + x_k) + \phi_c] e^{ju_0(x_l - x_k)}, \quad (1)$$

where

$$u_0 = \left(\frac{u_2 + u_1}{2}\right),$$

$$u_d = \left(\frac{u_2 - u_1}{2}\right),$$

$$\overline{|\eta_k^* \eta_l|} = \begin{cases} 0 \text{ for } l \neq k, \text{ and} \\ |\bar{\eta}_k|^2 \text{ for } l = k. \end{cases}$$

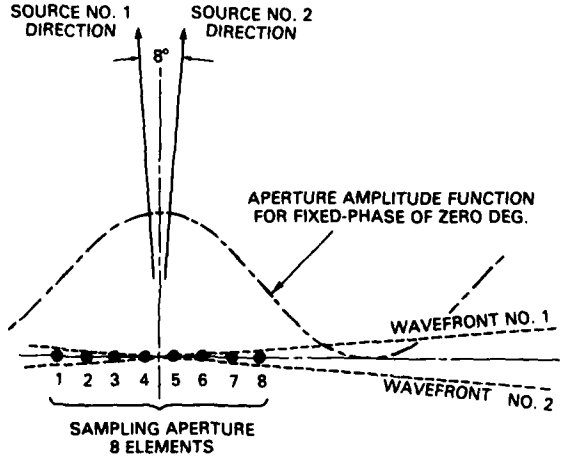

Fig. 1 — Aperture space modulation function produced by two equal-strength coherent sources located 8° apart in far field, linear-array sampling aperture of eight elements with half-wavelength spacing

The first three terms are identical to those in the noncoherent case and, taken alone, they are stationary in space, because the only space dependency involved is the separation distance $(x_l - x_k)$. They are equivalent to the time-domain situation of two sinusoids plus noise, that is, the spatial angle $\sin(\theta)$ is the dual of frequency, and the element location x_k is the dual of time-sampling instants. However, the product term [the fourth term in Eq. (1)] has an amplitude cosine variation that is dependent on the sum of the distances $(x_l + x_k)$ and thus will not be stationary in space. There is no equivalent in the time domain. The addition of the three exponent terms for $l = k$ results in the *aperture amplitude function* of Fig. 1. If the coherent sources maintain their fixed-phase relationship, and if the eight-element sampling aperture does not move, then Eq. (1) will cause the resulting sample covariance matrix to be non-Toeplitz, that is, the matrix-element values along diagonals will differ in accordance with the cosine amplitude function. Furthermore, one will find that this matrix has only one unique eigenvalue, that is, the two sources are blended into a single unique eigenvector instead of the usual two. Another way of looking at it is that the two coherent sources are blended into a single "virtual source," which can be quite different from the point-source/plane-wavefront model that corresponds to an equivalent time-domain sinusoid.

These characteristics will usually result in very unsatisfactory performance from the processing algorithms listed above. A typical example is shown in Fig. 2, where we have two 30-dB coherent sources located at 16° and 24° (8° spatial separation), a fixed coherent phase difference of $\phi_{c2n} = 90°$, a number of snapshots $N = 1024$, and an eight-element linear-array sampling aperture. The beamwidth of our eight-element array is about 16°, so that the sources are separated by about a half-beamwidth. The algorithm employed in this example is referred to as the *SLC algorithm*, which is described in the appendix. Other examples may be found in Ref. 11. Note that the performance of the SLC algorithm in Fig. 2b is no better than a conventional beam which is scanned through the sources, Fig. 2a. At a value of $\phi_{c2n} = 180°$ (not shown), the SLC algorithm will indicate that two sources are present, but the locations are incorrect.

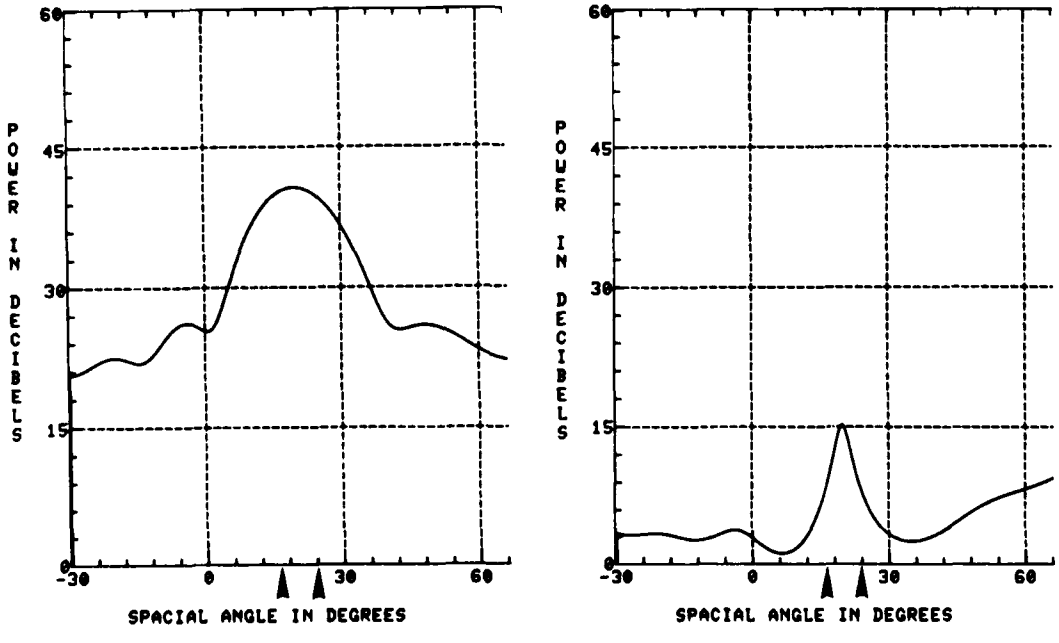

(a) Conventional beam scan

(b) SLC algorithm

Fig. 2 — Spatial spectrum estimates for 30-dB coherent sources, 90° phase, at 16° and 24° (8° apart), 8-element linear array, 1024 snapshots covariance matrix

Solutions to these difficulties may be found in those techniques which cause the product term in Eq. (1) to average near zero, so that the sample covariance matrix approaches the Toeplitz condition. For example, consider a sideways movement of the eight-element sampling aperture, such that the aperture line remains parallel for all snapshot positions. Note that, whenever we shift the position sideways between snapshots, we are changing the received phase difference between the two coherent sources, because the distances from the sources to the aperture phase center have changed. If we denote the incremental phase change per snapshot as $\Delta\phi_n$, then the coherent phase difference for the nth snapshot referenced to the aperture phase center may be written

$$\phi_{cn} = \phi_{c0} + \sum_{n=1}^{n} \Delta\phi_n, \tag{2}$$

where ϕ_{c0} is the starting phase difference. Thus, as we move sideways ϕ_{cn} changes with time, and each element samples the aperture-modulation function at different points as it moves along. After the sampling of one or more complete cycles of the modulation function, similar interelement-spacing covariance terms become approximately equal, the sample covariance matrix approaches the Toeplitz condition, and the resolution performance of the various algorithms becomes similar to their performance against noncoherent sources.

Some further thought on the time rate of change of ϕ_{cn} in Eq. (2) leads us quickly to the conclusion that we have formed a coherent doppler shift between the two sources via movement of the phase center of our sampling aperture. Furthermore, it is obvious that the identical result could be produced if we kept the position of the sampling aperture fixed but let the corresponding coherent doppler shift exist between the two sources. Note that, for Fig. 1, this would cause the aperture modulation function to move sideways with respect to the fixed sampling aperture. Thus, a doppler shift between coherent sources and targets gives us a second possibility for resolving them within a beamwidth. As indicated above, it is desirable to have enough snapshots to sample one or more complete doppler cycles so that the covariance matrix may approach the Toeplitz condition. Figure 3 illustrates the easy resolution of the same sources used in Fig. 2, except that source #2 is now given an incremental phase shift of $\Delta\phi = 1.1°$ per snapshot, so that it traverses 3.2 doppler cycles in the 1024 snapshots averaged for this particular case. The improvement is dramatic, and performance is fully equal to that in noncoherent cases. Experience has shown that performance is good whenever the doppler cyles exceed a value of about 0.75, with adequate sampling of the aperture-modulation envelope function.

FORWARD-BACKWARD SUBAPERTURE-SHIFT SOLUTION

If a doppler-cycle shift is not available, then we are forced to address the difficult fixed-phase coherent case. The best technique found to date is to form a reduced-dimension sample covariance matrix via synthetic shifting of a reduced-dimension sampling subaperture along the elements of the array. If L represents the number of elements in the sampling subaperture, and K is the total number of elements in our linear array antenna, then we can form a reduced $L \times L$ sample covariance matrix averaged over $(K - L + 1)$ samplings per array snapshot. Such synthetic movement of a subaperture is essentially a fractional doppler-cycle shifting of the source phasing at the phase center of the subaperture as it moves along the array. Furthermore, the averaging is usually improved significantly if our sampling subaperture is reversed and moves across the array in the opposite direction. This double synthetic sampling movement is illustrated in Fig. 4, where the reader will recognize its similarity to the forward-backward linear prediction techniques described in the literature [5,6]. Note that the resulting reduced $L \times L$ sample covariance matrix will be symmetric but still non-Toeplitz. Figure 5 illustrates the resolution of two 30-dB coherent sources spaced 4° apart for $L = 8$ and $K = 16$ elements, utilizing the SLC algorithm for various coherent fixed phases of 0, 10, 20, 90, 160, 170, and 180°.

Fig. 3 — Same coherent-source situation as in Fig. 2, except that doppler shift of 1.1° per snapshot is inserted

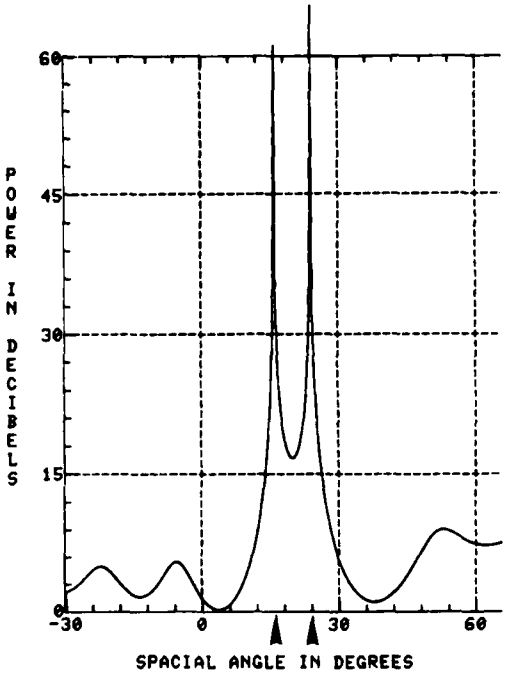

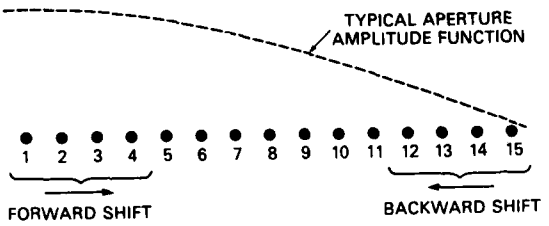

Fig. 4 — Illustration of forward-backward shift movement for a reduced-dimension sampling subaperture where $L = 4$, along a linear antenna array of $K = 15$ elements

Although it is not apparent in Fig. 5, there is a substantial performance dependency upon the fixed-phase difference between the two coherent sources. When $\phi_{c2n} = \pm 90°$, performance is about equal to that in the noncoherent case, because the forward-backward averaging effect is maximum. However, when $\phi_{c2n} = 0°$ or 180°, then the forward-backward averaging effect is minimum, because of the symmetry of the aperture-modulation envelope function, and performance suffers with respect to that in the noncoherent case.

The forward-backward subaperture-shift solution can also be applied to the single-snapshot case. Note that, when only one snapshot of data is available, we have a fixed-phase coherent case even if the sources are nominally noncoherent. The single-snapshot case is the most difficult of all, because the particular noise voltages frozen into that snapshot may have a large variance, bias offsets, or spurious peaks. To reduce the effects of the noise, it is always desirable to have a number of snapshots available for processing.

EIGENVALUE/EIGENVECTOR ALGORITHMS

When a signal is known to consist of pure sinusoids in white noise, an appropriate procedure to find the unknown frequencies and powers of the sinusoids in the signal is the Pisarenko spectral-decomposition procedure [14]. Much of the current interest in eigenvector methods can be traced to Pisarenko's work. Recent formulations specifically tailored to the spatial direction-finding problem have been described by Schmidt [7] and Bienvenu and Kopp [8]. These techniques are based upon the geometrical vector property that the "noise" eigenvectors of a covariance matrix are orthogonal to source direction vectors and, therefore, will produce zeros (nulls) at source locations.

The particular version used for processing the simulated snapshot data discussed in this report can be derived from the constrained optimized beam scan algorithm [1] or its identical counterpart, the

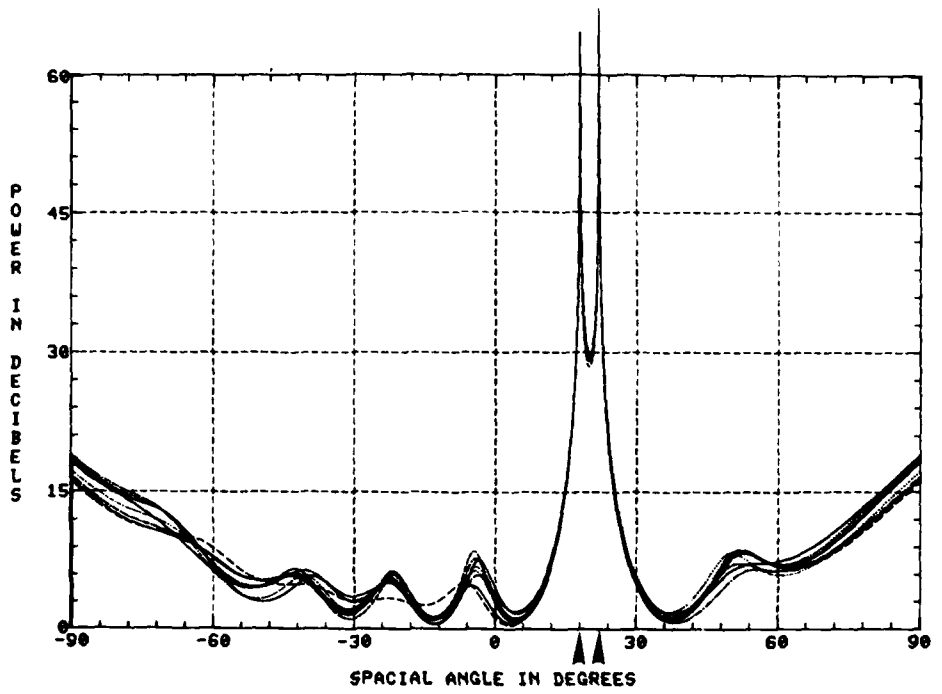

Fig. 5 — Spatial spectrum estimates for two 30-dB coherent sources located at 18° and 22° (0.5 beamwidths apart), 16-element linear array, 32 snapshots at each fixed-phase value of 0, 10, 20, 90, 160, 170, and 180° utilizing subaperture $L = 3$.

MLM algorithm of Capon and Lacoss [2], where the spatial spectrum would be estimated by the output residual power P_o from the optimized adapted array weights,

$$P_o = \mathbf{W}_o^{*\prime} \mathbf{M} \mathbf{W}_o, \tag{3}$$

where

$\mathbf{W}_o$ = optimized weights = $\mu \mathbf{M}^{-1} \mathbf{S}^*$,

$\mathbf{M}$ = covariance matrix estimate,

$\mathbf{S}^*$ = mainbeam direction steering vector, and

μ = a scalar quantity.

Under the zeroth-order gain constraint, we require that $\mathbf{S}' \mathbf{W}_o = 1$, whereupon

$$\mu = (\mathbf{S}' \mathbf{M}^{-1} \mathbf{S}^*)^{-1}. \tag{4}$$

Substituting μ and $\mathbf{W}_o$ into Eq. (3) then results in

$$P_o = \frac{1}{\mathbf{S}' \mathbf{M}^{-1} \mathbf{S}^*}. \tag{5}$$

If the steering vector $\mathbf{S}^*$ for a given covariance-matrix inverse is swept, P_o will estimate the spatial spectrum.

From the properties of the associated eigenvector orthonormal modal-matrix transformation, defined as the matrix **Q**, we can rewrite the covariance-matrix inverse in the form

$$\mathbf{M}^{-1} = \mathbf{Q}^{t}\left[\mathbf{Q}^{*}\,\mathbf{M}\,\mathbf{Q}^{t}\right]^{-1}\mathbf{Q}^{*} \tag{6}$$

$$= \mathbf{Q}^{t}\left[\frac{\delta ij}{\beta_i^2}\right]\mathbf{Q}^{*},$$

where β_i^2 is the ith eigenvalue of the covariance matrix. This then permits us to form a simple summation of eigenvector power beams referenced to the receiver noise-power level β_0^2,

$$\left[\frac{\beta_0^2}{P_o}\right] = \sum_{k=1}^{K}\left[\frac{\beta_0^2}{\beta_k^2}\right] g_k^2(\theta), \tag{7}$$

where

$$g_k(\theta) = \mathbf{S}^{t}\mathbf{e}_k. \tag{8}$$

The kth eigenvector beam, $g_k(\theta)$, is defined by the kth eigenvector $\mathbf{e}_k$. If we use all K beams, we have an identity with the constrained-optimized algorithm; but if we select only the noise eigenvector beams based upon a threshold criterion related to β_0^2, then we should get excellent nulls at all source positions, because the noise eigenvectors are orthogonal to the source direction vectors [7].

Under ideal simulation conditions, such as are assumed in this report, the threshold criterion is a simple set value, because the noise eigenvalues are well behaved and have a small spread in magnitude. However, in practical situations where system errors and imperfections tend to widen the spread in noise eigenvalues, one must develop a more sophisticated criterion tailored to the specific application.

An additional dividend from this algorithm is that, once the locations of the sources are determined, then their relative strengths may be evaluated from Eqs. (5) or (7), that is, the MLM algorithm. This pseudo-linear superposition property is dependent upon the reciprocal of a matrix inverse being equal to the sum of the reciprocals of the constituent matrix inverses. Other power estimation techniques with better characteristics are available [7,13,14]. It should be pointed out that estimation of source power is a key issue in the use of high-resolution techniques to sort out and reject false peaks in the spectral estimates. This becomes especially important when only a few snapshots are available and the SNR is low.

RESOLUTION PERFORMANCE: MIXED MULTIPLE SOURCES

Multiple source situations which include both coherence and unequal strengths constitute an excellent vehicle for testing estimation algorithms, and Fig. 6 illustrates an example in which we attempt to estimate six sources using an eight-element linear-array sampling aperture. This particular test case includes two 10-dB sources 95% correlated, at −54° and −42° (0.57 beamwidths apart), and four noncoherent sources of −9-, 30-, 10-, and 20-dB strengths, located at 0°, 15°, 22°, and 30°. Note in Fig. 6a that the conventional beam scan (Fourier transform) is hopeless, as expected, because of its beamwidth and sidelobe limitations. In addition, the simple SLC algorithm has failed to resolve the highly correlated sources and the two weaker noncoherent sources located at 0° and 22°. However, in Fig. 6b the eigenanalysis algorithm has located all six sources correctly via the "noise eigenvectors" and, in addition, permits us to evaluate the relative strengths of the noncoherent sources. This algorithm has consistently demonstrated more than an order-of-magnitude improvement in SNR/resolution performance over the older SLC algorithm.

Figure 6c illustrates a typical disaster that occurs whenever one attempts to work with a Toeplitz matrix constraint (autocorrelation matrix) in a coherent source situation. Interestingly, not only is the coherent source information distorted, but the noncoherent source information is badly affected as well.

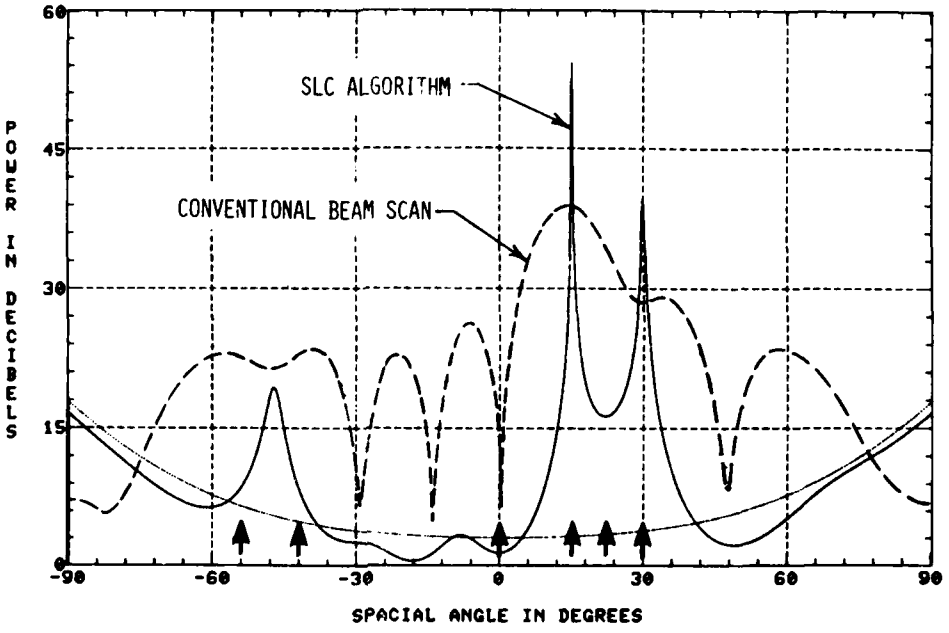

(a) Conventional/SLC algorithm

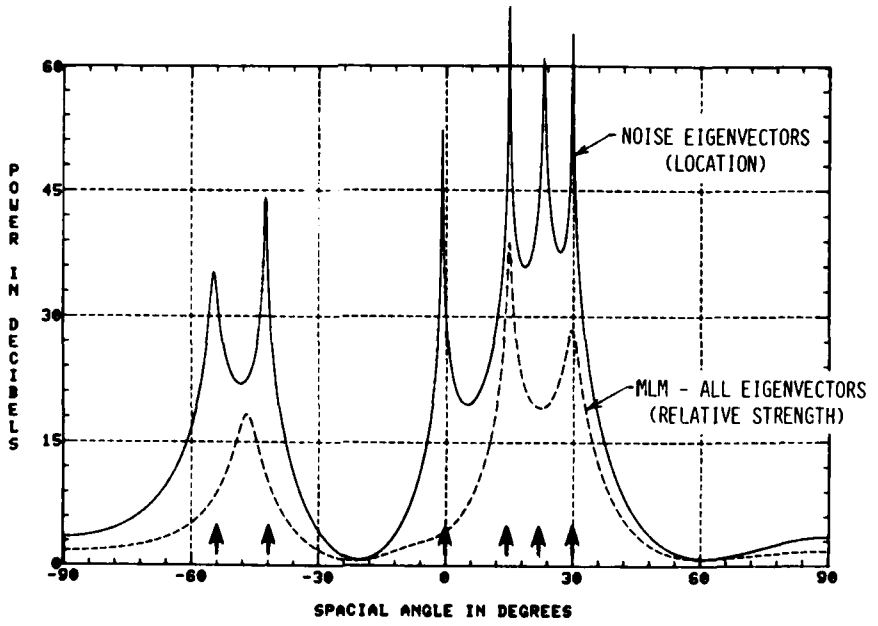

(b) Eigenvector algorithm, symmetric matrix constraint

Fig. 6 — Spatial spectrum estimate for six sources: two 10-dB sources 95% correlated at −54° and −42° (0.57 beamwidths apart); four noncoherent sources of −9-, 30-, 10-, and 20-dB strengths located at 0°, 15°, 22°, and 30°; 8-element linear array, sample covariance matrix of 1024 snapshots

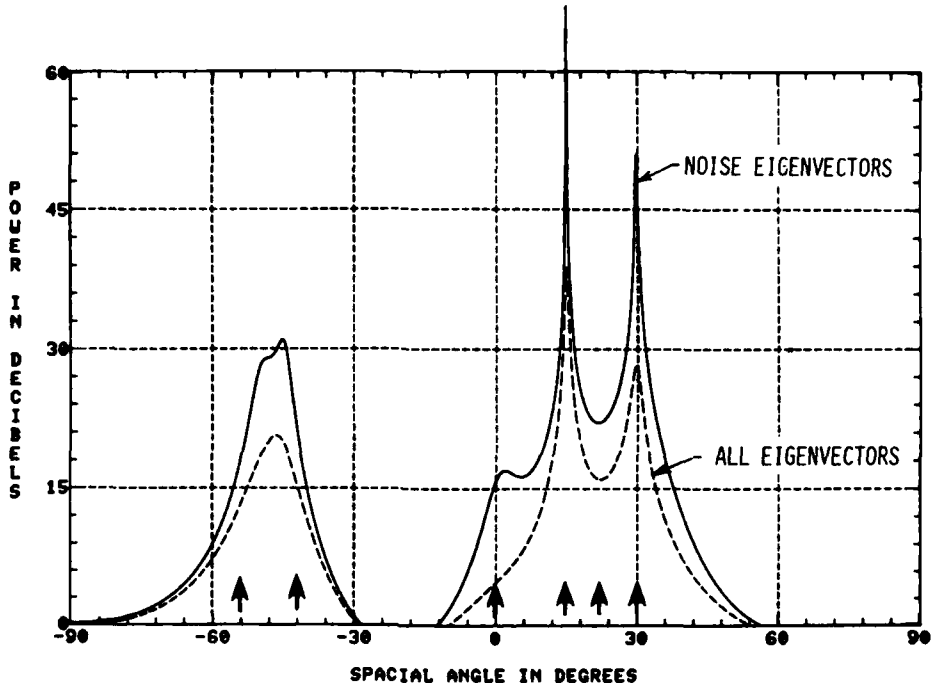

(c) Eigenvector algorithm, Toeplitz matrix constraint

Fig. 6 (Continued) — Spatial spectrum estimate for six sources: two 10-dB sources 95% correlated at −54° and −42° (0.57 beamwidths apart); four noncoherent sources of −9-, 30-, 10-, and 20-dB strengths located at 0°, 15°, 22°, and 30°; 8-element linear array, sample covariance matrix of 1024 snapshots

A MOVING-SOURCE TRACKING SIMULATION

The second example involves four moving sources, of unequal strength, traveling in criss-crossing patterns. The true paths for each source vs time are indicated in Fig. 7. Sources $S1$, $S2$, and $S3$ are coherent sources of low (−10-dB) strength: $S1$ is the reference source; $S2$ is 95% correlated, with a slow doppler shift of 0.027° per snapshot; and $S3$ is 95% correlated, with a moderate doppler shift of 0.586° per snapshot. Source J_0 is a noncoherent 20-dB source, intended to represent a strong jammer. The time scale of 90 units represents 59850 snapshots taken at equal sampling intervals, so that 665 snapshots are sampled within each time unit along the scale. Thus, for each time unit, source $S2$ advances 18° in phase and source $S3$ advances 390° in phase with respect to $S1$. The sampling aperture used in this example consists of a 12-element linear array with half-wavelength spacing.

A conventional Fourier-transform performance basis for this example is given in Fig. 8, where we have three different output display plots based upon scanning beam processing. Figure 8a illustrates a three-dimensional (3D) display output obtained from a conventional scanning beam of uniform illumination, identical to a Bartlett-window Fourier transform, wherein each time-unit plot cut is computed from the sample covariance matrix averaged over its 665 snapshots,

$$P_o = \mathbf{S}^{*t}\,\mathbf{M}\mathbf{S}, \tag{9}$$

where $\mathbf{M}$ is the sample covariance matrix and $\mathbf{S}$ is the beamsweep steering vector used to generate the display plot. As expected, this simple Fourier output is dominated by the strong source J_0 to such an extent that it is impossible to see the weak sources, let alone track them. If one attempts to utilize a

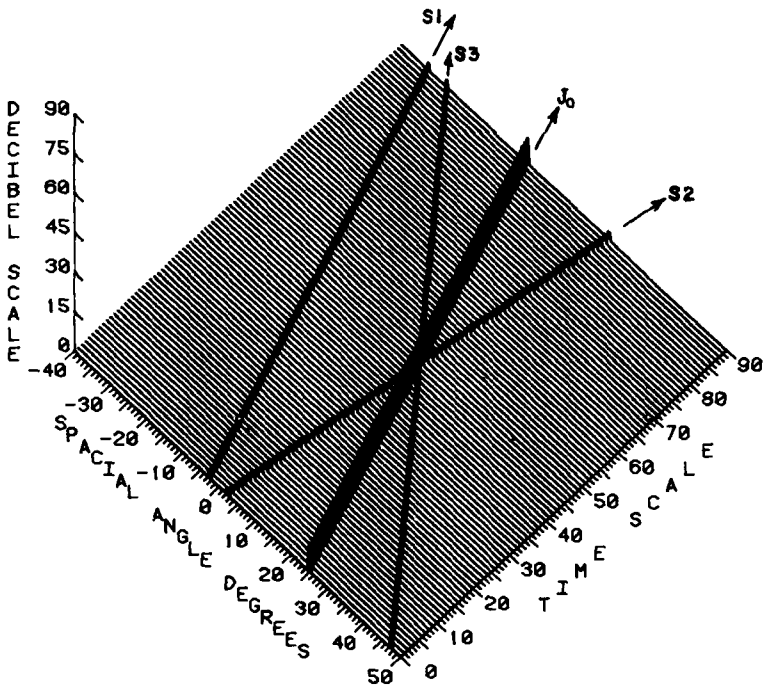

Fig. 7 — True paths used in tracking simulations for four moving sources; *S*1, *S*2, and *S*3 are coherent and of −10-dB strength; J_0 is a strong 20-dB noncoherent source

low-sidelobe window, as illustrated in Fig. 8b, the results are no better, because of the increase in beamwidth. Whenever one has a dominating strong-source situation like this, a good conventional technique to employ is pattern subtraction of the strong source, and Fig. 8c illustrates the considerable improvement available. Note that the paths of the three weak sources are now crudely outlined. Pattern subtraction is similar to the use of a spatial filter which nulls out the strong source. We need to know the direction angle, θ_0, of the strong source, and this can be obtained via automatic tracking of source J_0 in our example. Knowing θ_0, we can form a unit filter vector $\mathbf{F}_n$, where the kth element component may be written

$$F_{kn} = \frac{1}{\sqrt{K}} e^{ju_0 x_k}, \tag{10}$$

where

$$u_0 = \left(\frac{2\pi}{\lambda}\right) \sin \theta_0.$$

The correlation coefficient α_n between $\mathbf{F}_n$ and the snapshot signal-sample vector $\mathbf{E}_n$ defined in the appendix is given by

$$\alpha_n = \left[\mathbf{F}_n^{*t} \mathbf{E}_n\right]. \tag{11}$$

The filtered signal sample vector $\mathbf{E}_n'$ is then obtained by subtracting the filter direction components in Gram-Schmidt fashion, that is,

$$\mathbf{E}_n' = \mathbf{E}_n - \alpha_n \mathbf{F}_n. \tag{12}$$

From $\mathbf{E}_n'$ one can form the filtered sample covariance matrix $\mathbf{M}'$ and substitute into Eq. (9) to compute the time-unit plot cuts shown in Fig. 8c.

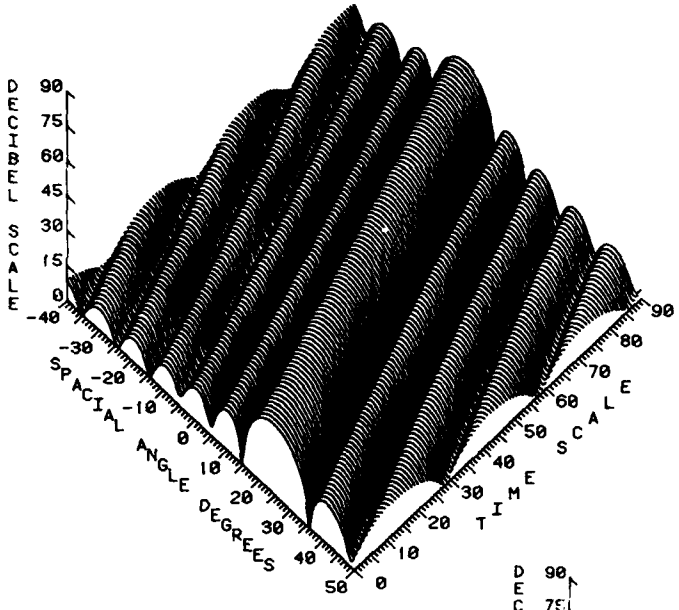

(a) Conventional scanned-beam (Fourier-transform) output with uniform element weights.

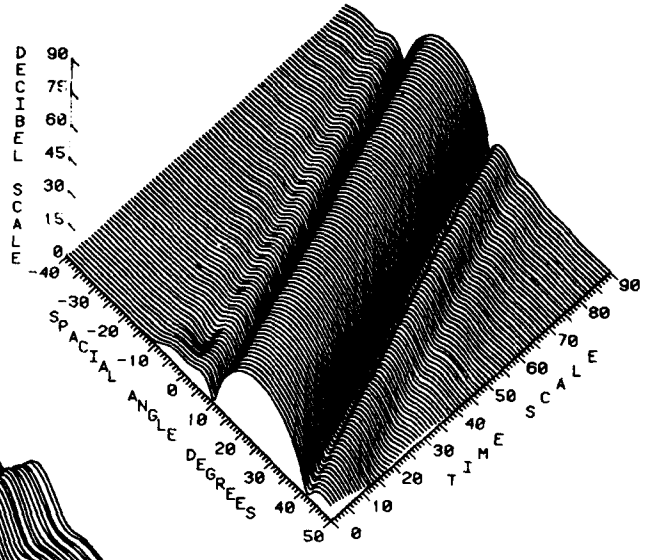

(b) Conventional scanned-beam (Fourier-transform) output with cosine-distribution element weights (first-sidelobe level of −24 dB).

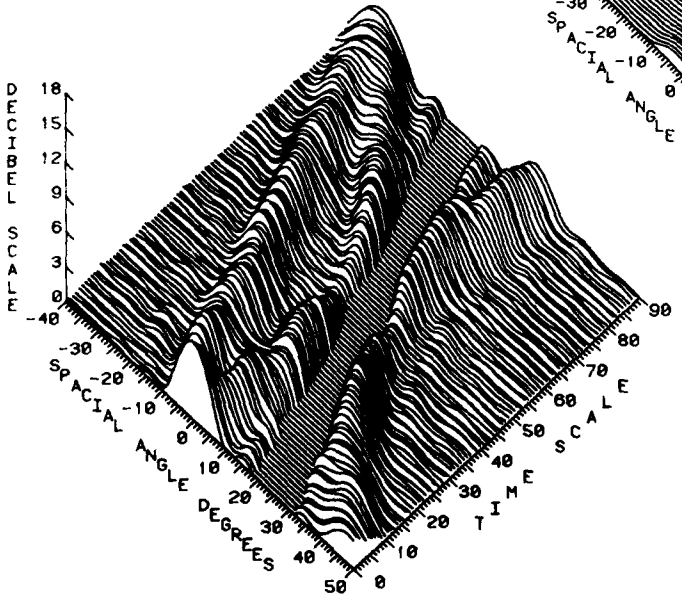

(c) Conventional scanned-beam (Fourier-transform) output, with uniform element weights, after notching-out strong source J_0 with an automatic spatial-tracking filter.

Fig. 8 — Tracking simulation displays for the four moving sources shown in Fig. 7; *S*1, *S*2, and *S*3 are coherent and of −10-dB strength; J_0 is a strong 20-dB noncoherent source; 12-element linear array sampling aperture; each time-unit plot cut is processed from 665 snapshots.

For comparison against the Fourier-transform processing results shown in Fig. 8, the results computed from eigenanalysis algorithm processing of the same snapshot data are illustrated in Fig. 9. In Fig. 9a, we have the 3D display computed from the full 12-element sample covariance matrix with no subaperture shift. Note that the correct tracks of all three weak sources are clearly indicated, even in the presence of the dominating strong source J_0. In addition, superresolution of these weak sources is evidenced in about 30% of the time display and contributes considerably to delineating the paths near crossovers.

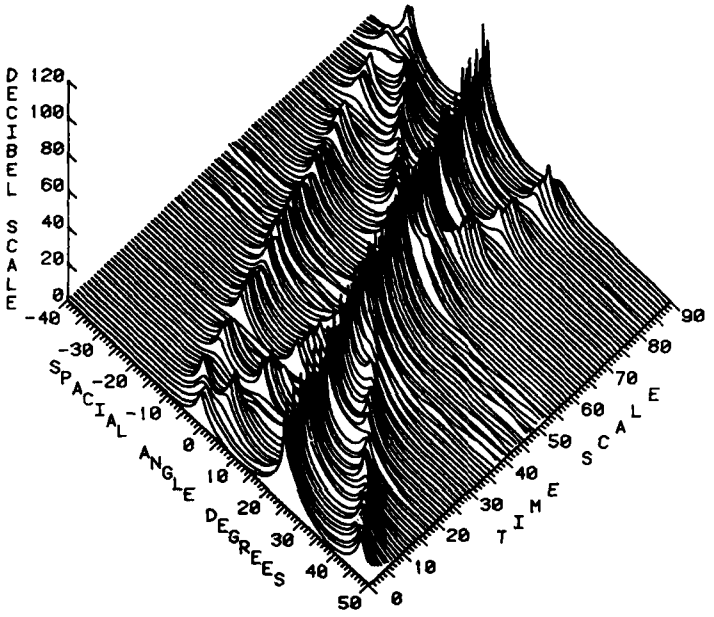

(a) No subaperture shift employed.

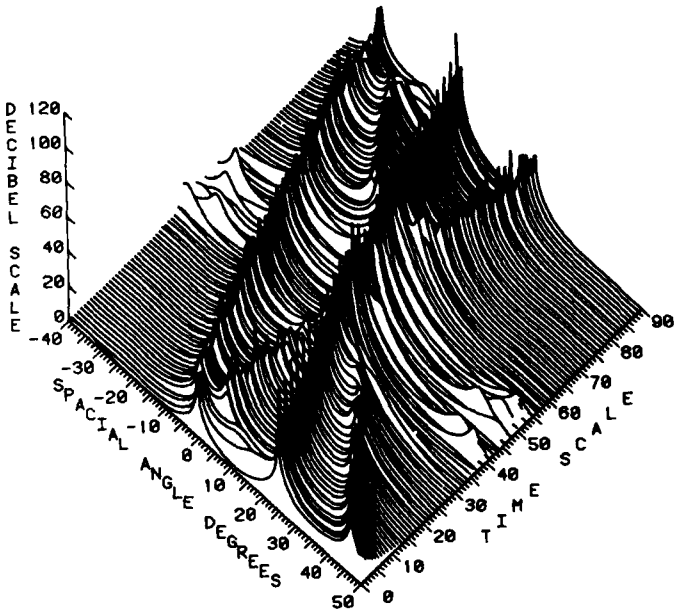

(b) Forward-backward subaperture-shift processing added, with subaperture $L = 8$ elements.

Fig. 9 — Eigenanalysis algorithm estimates for the four moving sources referenced in Fig. 8; same 12-element linear-array snapsnot data; each time-unit plot cut is processed from 665 snapshots.

It is of interest to note that sources $S1$ and $S2$ are not resolved for times $T = 0$, 1, and 2. The reason for this may be seen if we examine the coherent source information listed in Table 1, which shows that these two sources start out in phase at a separation of 0.5 beamwidths. There is a noticeable peak modulation along the paths of $S1$ and $S2$, corresponding to the slowly changing phase difference between them. This modulation persists even when they are separated by several beamwidths.

Table 1 — Coherent Sources $S1$ and $S2$

Time T	Spacing $\Delta\theta_a$ (beamwidths)	Average Phase Difference $\Delta\phi$ (deg)
0	0.50	0
1	0.55	18
2	0.60	36
3	0.65	54
4	0.70	72
5	0.75	90
6	0.80	108
7	0.85	126
8	0.90	144
9	0.95	162
10	1.00	180

The 3D display output can usually be improved significantly for coherent sources by the incorporation of some forward-backward subaperture-shift processing, as described earlier. Figure 9b illustrates this improvement for the current example, with a subaperture of eight elements used to process the same 12-element data snapshots. Note that not only are the peaks higher and cleaner, but the modulation of the peak amplitudes referred to above has been largely eliminated.

Thus far in this final example, each plot cut was processed from the full 665 snapshots per time unit. If we reduce the number of snapshots processed, then the averaging in the sample covariance matrix is proportionally reduced, the variance of our estimates increases, and false alarms or spurious estimates will increase. In brief, the 3D display output will tend to become noisy. Figure 10 illustrates this noisy effect caused by a reduction to only 32 snapshots processed per time unit. Note that the track of the strong source J_0 is not bothered much by the reduction, because of its high SNR.

More dramatic differences between conventional Fourier transform processing and eigenanalysis processing could readily be demonstrated by an increase in the strengths of sources $S2$ and $S3$ in our example or by the the addition of more sources of unequal strengths.

CONCLUSIONS

Current spectral-estimation techniques have been applied to multiple-source situations, which include both coherence and unequal strengths, in cases designed to illustrate two of the important performance characteristics of interest in radar or passive tracking: superresolution and apparent absence of sidelobes. The simulations demonstrate a resolution capability that is very impressive compared to conventional techniques, and they have optimistic implications regarding the simultaneous accurate tracking of closely spaced, mixed, multiple sources or targets. In addition to these results, recent work reported by other researchers [13] also indicates that the level of performance achieved with modern spectral-estimation techniques has reached the point where these techniques invite in-depth consideration for real-world tracking-system applications.

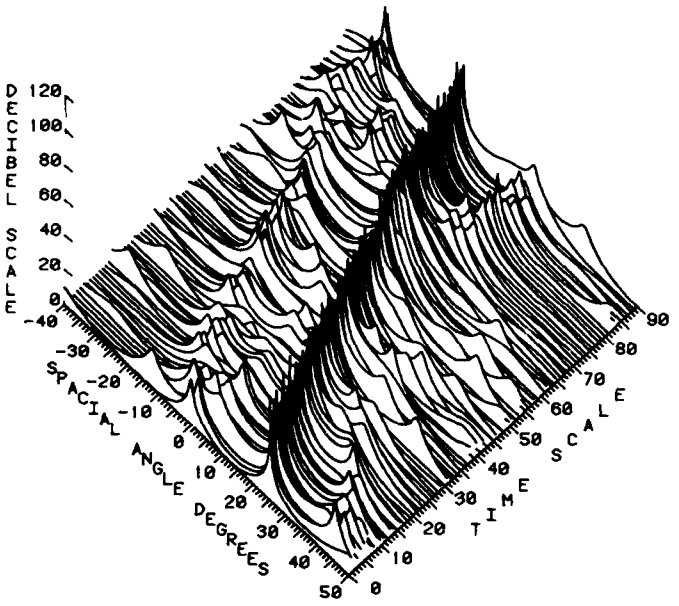

Fig. 10 — Eigenanalysis algorithm estimates with the same processing as Fig. 9b, except that the number of snapshots processed per time-unit plot cut is reduced to 32

It is recognized that a number of serious issues and problem areas remain to be addressed. For example:

- The basic reliability of source or target location in a statistical sense under practical tracking conditions. This includes threshold criteria and false alarm problems.
- The compatibility of mixing with conventional range and doppler signal processing to achieve improved four-dimensional radar space-resolution performance.
- The robustness of the model-dependent data-adaptive processing when the source scenario exceeds the available degrees of freedom, causing saturation degradation.
- The basic array and channel error and accuracy considerations. This includes the often-overlooked requirement for calibration of the element or beam patterns for all scan angles and bandwidths.
- The extensive impact upon overall system design, from the antenna to the interactive output display. An all-digital system is clearly indicated.
- The cost effectiveness compared to conventional techniques.

Obviously, considerable research effort is required to achieve the desired goals, but the outlook is optimistic because of the rate of progress which has characterized these techniques in recent years.

ACKNOWLEDGMENT

The 3D display plots contained in this report were produced via subroutine Fortran IV codes developed by H. Paris Coleman [15].

REFERENCES

1. W.F. Gabriel, "Spectral Analysis and Adaptive Array Superresolution Techniques," *Proc. IEEE* **68**, 654-666 (June 1980).

2. D.G. Childers, ed., *Modern Spectrum Analysis*, IEEE Press, New York, 1978.

3. R.A. Monzingo and T.W. Miller, *Introduction to Adaptive Arrays*, John Wiley & Sons, New York, 1980.

4. M.A. Alam, "Orthonormal Lattice Filter—A Multistage Multichannel Estimation Technique," *Geophysics* **43**, 1368-1383 (Dec. 1978).

5. A.H. Nuttall, "Spectral Analysis of a Univariate Process with Bad Data Points, via Maximum Entropy and Linear Predictive Techniques," NUSC-TR-5303, Naval Underwater Systems Center, New London, Mar. 1976.

6. L. Marple, "A New Autoregressive Spectrum Analysis Algorithm," IEEE *Trans. Acoust., Speech, Signal Process.* **ASSP-28**, 441-454 (Aug. 1980).

7. R. Schmidt, "Multiple Emitter Location and Signal Parameter Estimation," *Proceedings of the RADC Spectrum Estimation Workshop*, RADC-TR-79-63, Rome Air Development Center, Rome, N.Y., Oct. 1979, p. 243.

8. E. Bienvenu and L. Kopp, "Adaptive High Resolution Spatial Discrimination of Passive Sources," *Underwater Acoustics and Signal Processing*, D. Reidel Publishing Co., Boston, 1981, pp. 509-515.

9. S.M. Kay and S.L. Marple, Jr., "Spectrum Analysis—A Modern Perspective," *Proc. IEEE* **69**, 1380-1419 (Nov. 1981).

10. J.E. Evans, "Aperture Sampling Techniques for Precision Direction Finding" and "Comments on 'Angular Spectra in Radar Applications'," *IEEE Trans. Aerosp. Electron. Syst.* **AES-15**, 891-895 and 899-903 (Nov. 1979).

11. W.D. White, "Angular Spectra in Radar Applications," *IEEE Trans. Aerosp. Electron. Syst.* **AES-15**, 895-899 (Nov. 1979).

12. T. Thorvaldsen, "A Comparison of the Least Squares Method and the Burg Method for Autoregressive Spectral Analysis," *IEEE Trans. Antennas Propag.* **AP-29**, 675-679 (July 1981).

13. J.E. Evans, J.R. Johnson, and D.F. Sun, "High Resolution Angular Spectrum Estimation Techniques for Terrain Scattering Analysis and Angle of Arrival Estimation," *Proceedings of the First ASSP Workshop on Spectral Estimation*, McMaster University, Hamilton, Ontario, Canada, Aug. 1981, Vol. 2, pp. 5.3.1-5.3.10.

14. V.F. Pisarenko, "The Retrieval of Harmonics from a Covariance Function," *Geophys. J. (Royal Astron. Soc.)* **33**, 347-366 (1973).

15. H.P. Coleman, "A Fortran IV Plot Routine with Hidden Line Suppression for Use with Small Computer Systems," NRL Memorandum Report 4776, Mar. 26, 1982.

Appendix
SIGNAL SAMPLES AND SLC ALGORITHM

Consider a simple linear array of K equally spaced elements. The received-signal samples will be correlated in both space and time, giving rise to a two-dimensional data problem, but we convert this to the spatial domain only by assuming that narrowband filtering precedes our spatial-domain processing. Signal samples are defined as aperture snapshots, that is, one simultaneous sampling of the aperture signals at all array elements. The nth snapshot signal sample at the kth element will consist of independent Gaussian receiver noise, η_{kn}, plus the two coherent source voltages,

$$E_{kn} = \eta_{kn} + A_1 e^{j\psi_{1kn}} + A_2 e^{j\psi_{2kn}}, \tag{A1}$$

where

$$\psi_{ikn} = [u_i x_k + \phi_{cin} + \phi_{rn}],$$

$$u_i = \frac{2\pi}{\lambda} \sin \theta_i,$$

and λ = wavelength, x_k = position of kth element from center in wavelengths, θ_i = spatial location of ith source, A_i = amplitude of ith source, ϕ_{rn} = random-sampled phase of both sources for the nth snapshot, $\phi_{c1n} = 0$ so that source #1 becomes our coherent-source reference, and ϕ_{c2n} then incorporates the coherent phase difference between the two sources. A nontrivial point is that the coherent phase difference is referenced to the center of the array.

A convenient vehicle for application of the matrix-inverse type of algorithm is the generic SLC (sidelobe-canceler) antenna configuration illustrated in Fig. A1. The reader will note its resemblance to a linear prediction filter [1]. Throughout the report, this configuration is referred to simply as the *SLC algorithm*. The spatial spectrum estimates are the reciprocals of the adaptive-filter patterns, which, in turn, are computed from the optimum weights, $\mathbf{W}_o$. We simply compute $\mathbf{W}_o$ from the inverse of the sample covariance matrix [3],

$$\mathbf{W}_o = \mu \mathbf{M}^{-1} \mathbf{S}^*, \tag{A2}$$

$$\mathbf{S}^{*t} = [0, 0, 0, 0, 0, 0, 0, 1], \tag{A3}$$

$$\mathbf{M} = \frac{1}{N} \sum_{n=1}^{N} \mathbf{M}_n, \tag{A4}$$

and

$$\mathbf{M}_n = [\mathbf{E}_n^* \mathbf{E}_n^t], \tag{A5}$$

where $\mathbf{E}_n$ is the nth snapshot signal-sample vector, whose element components are given by Eq. (A1), $\mathbf{M}_n$ is the nth snapshot contribution to the covariance matrix, $\mathbf{M}$ is the sample covariance matrix averaged over N snapshots, $\mathbf{S}^*$ is the quiescent-weight steering vector, and μ is a scalar quantity. Note that, in true sidelobe-canceler fashion, the steering vector $\mathbf{S}^*$ injects a zero weight on every element except for the end element, thus causing the quiescent pattern of the array to be that of the single end element. Several examples of the use of this SLC algorithm against noncoherent sources can be found in Ref. [1].

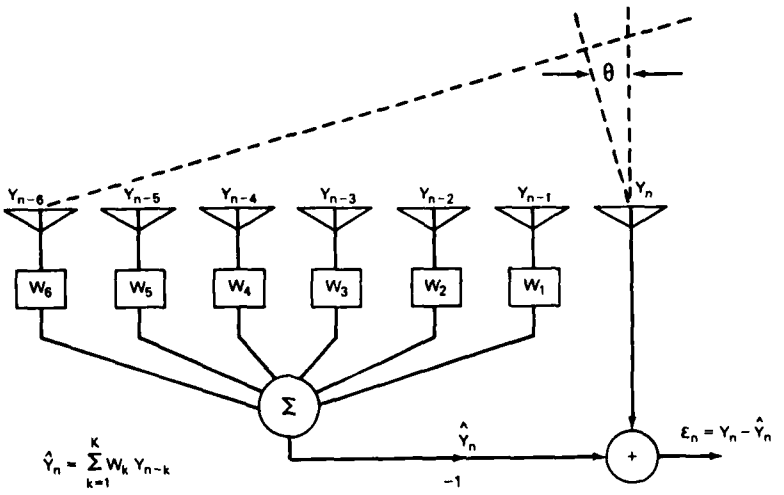

Fig. A1 — Array-aperture SLC algorithm configuration


DATE
ILME
8